

# Bi vacancy formation in BiFeO<sub>3</sub> epitaxial thin films under compressive (001)-strain from first principles

Lu Xia,<sup>a</sup> Thomas Tybell<sup>b</sup> and Sverre M. Selbach<sup>a</sup>

Point defects in BiFeO<sub>3</sub> affect both structural and functional properties. To elucidate the role of single Bi vacancies and Bi-O vacancy pairs we investigate their stability and effect on structural and ferroelectric properties in BiFeO<sub>3</sub> using first principles density functional theory calculations. Compressive strain is shown to stabilize Bi vacancies, and the Bi vacancy enthalpy of formation drops abruptly at the structural transition from rhombohedral R-phase to tetragonal T-phase. For Bi-O vacancy pairs the situation is more complex, albeit stabilization is found under compressive strain. Out-of-plane oriented vacancy pairs are stabilized in the T-phase, while in-plane oriented vacancy pairs are destabilized compared to the R-phase. It is shown that single Bi vacancies do not affect the spontaneous polarization, while in-plane Bi-O vacancy pairs reduce the in-plane component of the polarization, resulting in a polarization rotation towards [001]. We also discuss the effect of vacancies on the electronic properties of BiFeO<sub>3</sub>, and show that Bi deficiency is consistent with the experimentally reported *p*-type conductivity.

## 1 Introduction

BiFeO<sub>3</sub> (BFO) is a multiferroic with ferroelectric ( $T_C \approx 830$  °C) and antiferromagnetic ( $T_N \approx 370$  °C) order above room temperature.<sup>1</sup> Epitaxial thin films currently hold promise for technological applications in information storage and spintronics.<sup>2</sup> However, the properties and crystal structure are strongly influenced by epitaxial strain<sup>3-6</sup>, and the local defect structure.<sup>7,8</sup> Bulk BFO is a rhombohedral perovskite with space group  $R3c$  below  $T_C$ .<sup>9</sup> In bulk, the spontaneous polarization of  $\sim 90 \mu\text{C}/\text{cm}^2$ , mainly driven by  $6s^2$  lone-pairs on Bi<sup>3+</sup> cations, points along the pseudocubic [111] axis.<sup>10</sup> Antiferrodistortive rotations of the FeO<sub>6</sub> octahedra about the same [111]<sub>pc</sub> axis results in a  $a^-a^-a^-$  Glazer tilt system.<sup>11,12</sup> Due to the flexible crystal structure, BFO can be grown on a variety of oxide substrates, with a large range of possible epitaxial strain values.<sup>3-5</sup> Zeches *et al.* demonstrated that (001)-strained BFO thin films change their symmetry from rhombohedral with a small monoclinic distortion (“R-phase” or “R”) to a monoclinic tetragonal-like phase (“T-phase” or “T”) at compressive strains exceeding 4.5%.<sup>13</sup> The strain-stabilized T-phase has a large tetragonality ( $c/a = 1.25-1.3$ ), a strongly enhanced polarization of  $\sim 150 \mu\text{C}/\text{cm}^2$  and a strong piezoelectric response.<sup>13-16</sup>

Point defects are expected to affect properties like crystal structure, polarization, dielectric constant, magnetization and leakage current, but are difficult to study experimentally in thin films.<sup>7,8,17-21</sup> It is challenging to prepare stoichiometric BFO thin films, and large compositional deviations have been reported for single-phase materials.<sup>7</sup> Epitaxial strain has been demonstrated to strongly affect the point defect concentration in transition metal oxide thin films in recent years, but most work has been devoted

to oxygen rather than cation vacancies.<sup>22-26</sup> However, as Bi is a volatile element, Bi stoichiometry is challenging to control during synthesis and processing,<sup>27-31</sup> particularly of thin films. Although the defect chemistry of bulk BFO has been studied by DFT,<sup>32-40</sup> a fundamental understanding of the interplay between cation vacancy formation, epitaxial strain, and physical properties is still lacking.

Here we use Density Functional Theory (DFT) calculations to investigate the effect of epitaxial strain on the formation of Bi vacancies and Bi-O vacancy pairs in (001) strained BFO over a wide range of strain from zero to 6% compressive strain. Stabilization of Bi vacancies and Bi-O vacancy pairs under compressive strain is predicted, while the energetically favored orientation of vacancy pairs changes upon crossing the R-phase to T-phase boundary. The effect of Bi deficiency on polarization and electronic structure is discussed and compared to recent experimental reports.

## 2 Computational details

Density functional theory calculations were performed with the projector-augmented wave (PAW) method using the Vienna *Ab-initio* Simulation Package (VASP 5.3) and the PBEsol functional.<sup>41-44</sup> An effective U of 4 eV was applied to the strongly correlated Fe 3d electrons,<sup>45, 46</sup> which were initialized with collinear G-type antiferromagnetic order in all calculations. Plane waves were expanded up to a cutoff energy of 550 eV and the Bi\_d, Fe\_pv and standard O pseudopotentials supplied with VASP were used.

Pseudo-cubic 40-atom unit cells were used to model the *R3c* bulk ground state, while both 40-atom and 320-atom supercells were used for defect calculations. One Bi atom was removed from the cell to create one Bi vacancy, resulting in defect concentrations of 12.5% and 1.56% for the 40- and 320- atom cells, respectively. The calculated formation enthalpy of a Bi vacancy differed by only 0.02 eV between the 40 and 320 atom cells. Hence, the 40 atom cells were used to calculate strained defect cells. We note that substantial Bi deficiency is not unrealistic in BiFeO<sub>3</sub>.<sup>7, 31</sup> Reciprocal space integration was performed with a 3×3×3 gamma-centered k-point mesh for the 40-atom cell. Ferroelectric polarization was calculated by the Berry phase method for stoichiometric cells,<sup>47</sup> while the point charge method was used for defect cells.

Epitaxial strain was calculated as  $(a_{ps}-a_{0,ps})/a_{0,ps} * 100\%$ , where  $a_{0,ps}$  is the relaxed in-plane lattice parameter of unstrained bulk. Biaxial epitaxial strain in the (001) plane was imposed by fixing the in-plane lattice constants while relaxing the out-of-plane lattice constant and all ionic positions for stoichiometric cells.<sup>48</sup> To determine the R-phase to T-phase crossover in stoichiometric cells, we varied the out-of-plane lattice parameter for each strain level and optimized the atomic positions. For defect calculations, all three lattice vectors were fixed while the ionic positions were relaxed until the Hellman-Feynman forces on the ions were less than 0.01 eV/Å. Test calculations with point defects, allowing the lattice vectors to relax, gave the same cross-over strain value between the R- and the T-phase.

The Bi vacancy formation enthalpy,  $E_{V_{Bi}}$ , in a neutral cell was calculated as:

$$E_{V_{Bi}} = E_{tot,V_{Bi}} - E_{tot,stoich} + \mu_{Bi} \quad (1)$$

where  $E_{tot,V_{Bi}}$  and  $E_{tot,stoich}$  are the total energies of the defect cell and the perfect cell, respectively, and  $\mu_{Bi}$  is the chemical potential of Bi. The formation enthalpy of a Bi-O vacancy pair was calculated by adding the chemical potential of O,  $\mu_O$ , to eq. (1). The chemical potentials for Bi and O were determined by considering the different chemical reactions between the binary Bi and Fe oxides, using the calculated total energies of the following reference materials: Bi ( $R-3m$ , 166), Fe ( $Im-3m$ , 229),  $Bi_2O_3$  ( $P2_1/c$ , 14), FeO ( $Fm-3m$ , 225),  $Fe_3O_4$  ( $Fd-3m$ , 227),  $Fe_2O_3$  ( $R-3c$ , 167) and  $O_2$  (molecule in orthorhombic cell). The oxygen rich and oxygen poor limits of -5.41 and -7.29 eV, respectively, were determined using the equilibria  $O_2/Fe_2O_3/BiFeO_3$  and  $Bi/Bi_2O_3/BiFeO_3$ , respectively. The total energies of the reference compounds were obtained after full geometry optimization using the same computational parameters for consistency, and with Hubbard U corrections for iron containing compounds following Jain *et al.*<sup>49</sup> Magnetic orders of iron containing compounds were adopted from literature.<sup>50</sup>

### 3 Results and discussion

#### 3.1 Compressive strain induced “R” to “T” transition in stoichiometric BFO

Before addressing the effects of point defects, we first reproduce the isosymmetric phase transition induced by (001) epitaxial strain in stoichiometric cells. The crossover from R-phase to T-phase occurred at 4.5% compressive strain, in agreement with previous experimental and computational work.<sup>13,14</sup>

To gain insight into the structural response to strain, we present key structural parameters in Fig. 1. The  $c/a$  ratio goes through a discontinuous step at 4.5% compressive strain from 1.15 on the R side to 1.24 on the T side (Fig. 1(a)), accompanied by an 8% volume increase (Fig. 1(b)) and an abrupt loss of octahedra rotations about the out-of-plane axis (Fig. 1(c)). Rectification of the octahedral tilts about the [001] axis mitigates stretching of the Fe-O bonds upon the transition from R- to T-phase, whilst the size mismatch of the  $AO_{12}$  dodecahedron relative to the  $BO_6$  octahedron, quantified by the polyhedral volume ratio  $V_A/V_B$ ,<sup>51,52</sup> increases from 4.66 to 4.90 across the R to T boundary (Fig. 1(d)). A Fe displacement towards one of the apical oxygens also serves as a moderation mechanism of the lattice distortion. Large polar displacements of Fe from the octahedral centers, depicted in Fig. 1(e), give rise to a significant enhancement of the out-of-plane polarization, effectively rotating the polarization direction from  $[111]_{pc}$  to  $[001]_{pc}$  (Fig. 1(e-f)). Fig. 1(f) shows that the in-plane polarization is suppressed by decreasing the in-plane lattice parameters, while the overall polarization of  $155\mu C/cm^2$  of the T-phase at 4.5% compressive strain is larger than reported for bulk materials.<sup>1,2,14</sup>

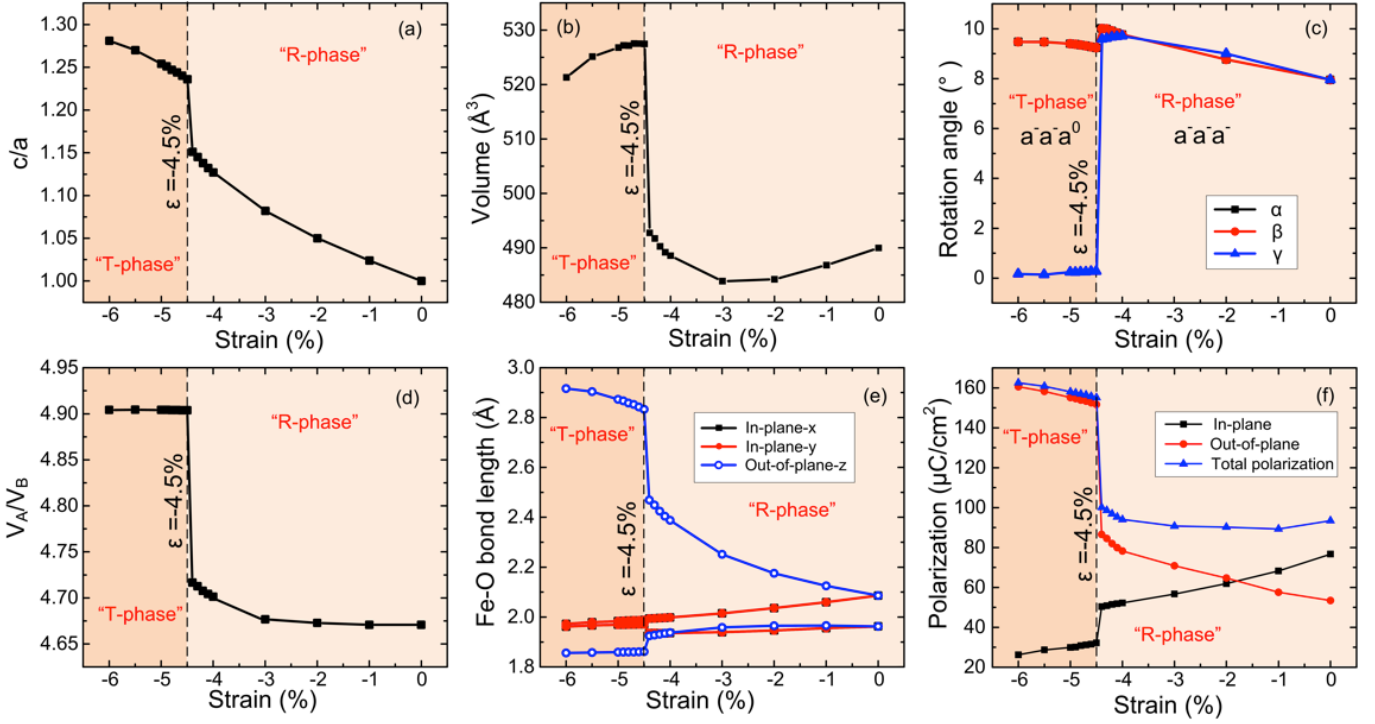
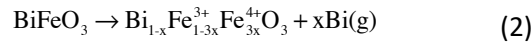


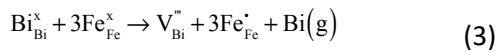
**Fig. 1** Variation of structural parameters of  $\text{BiFeO}_3$  as a function of (001)-strain. (a)  $c/a$  ratio for a 40-atom pseudocubic cell; (b) volume of the 40-atom pseudocubic cells; (c) rotation angles of the  $\text{FeO}_6$  octahedral around the three principal lattice vectors; (d) polyhedral volume ratio  $V_A/V_B$ ; (e) Fe-O bond lengths of the oxygen octahedra; (f) total polarization and in-plane and out-of-plane polarization components.

### 3.2 Strain dependence of Bi vacancy formation energy

First the effect of a large defect concentration, 12.5%, was investigated with one Bi-vacancy in the 40-atom cell (Fig. 2(a-b)). Under oxygen rich conditions, Bi vacancies can form by evaporation of gaseous Bi (g) through the reaction:



The electronic charge compensation by holes of a Bi vacancy can be formally expressed by the Kröger-Vink equation:



where  $\text{Bi}_{\text{Bi}}^x$  and  $\text{Fe}_{\text{Fe}}^x$  are  $\text{Bi}^{3+}$  and  $\text{Fe}^{3+}$  in their regular lattice sites,  $V_{\text{Bi}}^{\bullet\bullet\bullet}$  is a bismuth vacancy of relative charge -3 and  $\text{Fe}_{\text{Fe}}^{\bullet}$  is  $\text{Fe}^{4+}$ .<sup>30</sup> The calculated formation energy of a Bi vacancy in unstrained bulk is 5.43eV. Interestingly, the strain induced transition from the R- to the T-phase at 4.5% compressive strain is not affected by the presence of a Bi vacancy, as illustrated in Fig. 2(c). This can be rationalized from the subtle

differences between the local structure around a vacancy compared to the perfect rhombohedral and tetragonal structures.

The formation enthalpy of a Bi vacancy decreases monotonically with increasing compressive strain, displaying a minimum value in the R-phase at  $\sim 3.5\%$  compressive strain, before increasing upon further compressive strain towards the R to T transition (Fig. 2(c)). This increase may stem from the non-linear evolution of polar cation displacements and octahedral rotations under strain. As the strain increases towards the phase boundary, polar cation displacements perpendicular to the strain plane become more favored while out-of-plane octahedral rotations are suppressed. This structural strain mitigation mechanism becomes increasingly less energetically favourable beyond 3.5% strain until entering the T-phase, where a completely different rotation mode is adopted.

Upon entering the T-phase, Bi vacancies are stabilized by 0.12 eV compared to in the R-phase, and the formation enthalpy continues to decrease monotonically with increasing compressive strain. The formation enthalpy of Bi vacancies in the T-phase is thus larger than a simple extrapolation from the “R-phase” would suggest. The maximum formation enthalpy in the T-phase at  $-4.5\%$  strain is comparable to the minimum value found in the R-phase at  $-3.5\%$  strain.

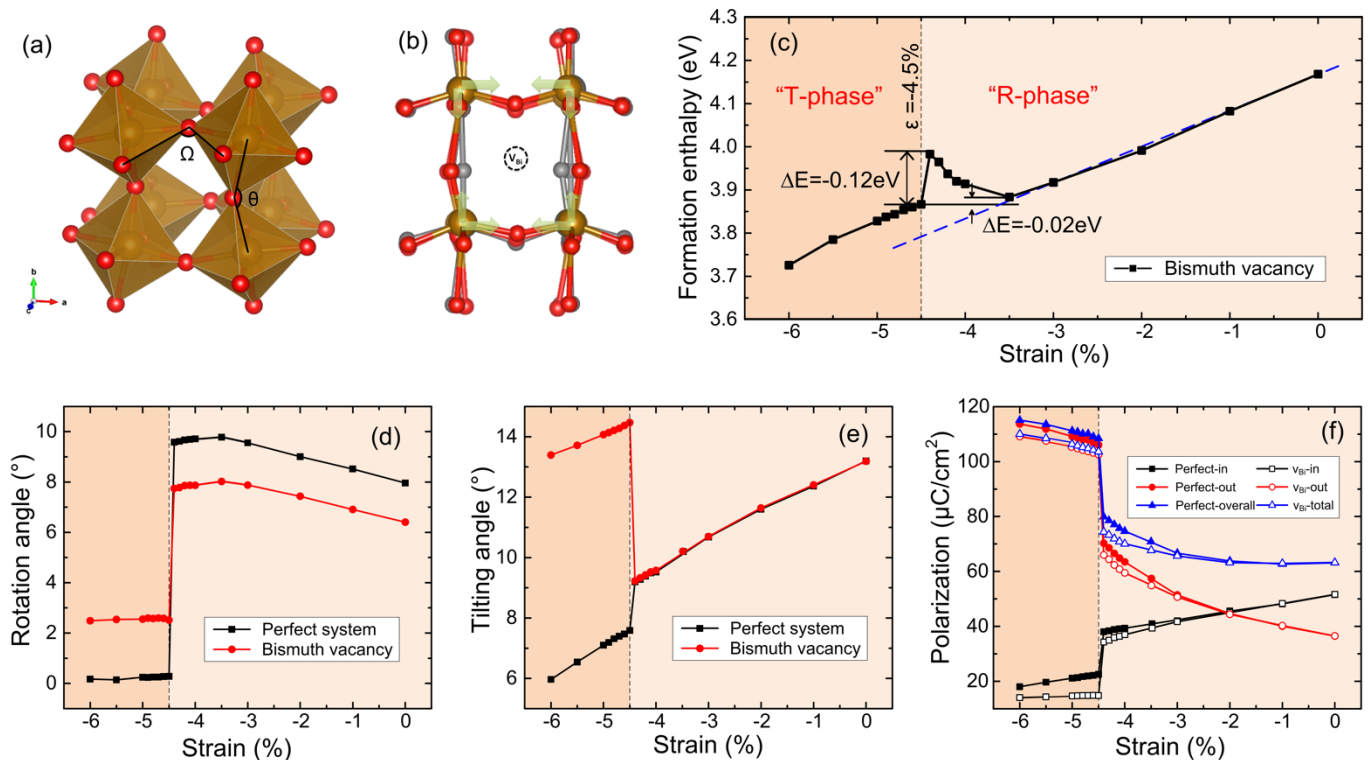


**Fig. 2** Bismuth vacancy formation in (001)-strained  $\text{BiFeO}_3$ . (a) Crystal structure of rhombohedral  $R3c$   $\text{BiFeO}_3$  with rotation ( $\Omega$ ) and tilting ( $\theta$ ) angles defined. (b) Structural relaxation around a Bi vacancy in the T-phase. Coloured atoms show the relaxed structure with a Bi vacancy, grayscale atoms behind show the pristine structure. Green arrows indicate Fe displacements. (c) Bi vacancy enthalpy of formation as a function of compressive strain. (d) Octahedral rotation angle  $\Omega$ , (e) octahedral tilting angle  $\theta$  and (f) point charge model calculated polarization components as a function of compressive strain for  $\text{BiFeO}_3$  with and without a Bi vacancy.

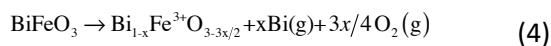
### 3.3 Local structural response to Bi vacancies under strain

Rotation and tilting of oxygen octahedra affect the orbital overlap between Fe 3d and O 2p, and thus the electronic properties. We define the rotation around the z axis (out-of-plane) separately from those around the x and y axes, which are referred to as tilting angles. The rotation and tilting angles defined by the angles  $\Omega$  and  $\theta$ , respectively, where  $\Omega$  is the angle between the edges of two corner sharing octahedra, while  $\theta$  is the angle along the Fe-O-Fe bond, as illustrated in Fig. 2(a). The rotation and tilting angles are defined by the relations  $(90^\circ - \Omega)/2$  and  $(180^\circ - \theta)/2$  respectively. For stoichiometric BFO, in the R-phase an increasing rotation angle and decreasing tilting angle under compressive strain mitigates the Fe-O bond compression when the in-plane lattice parameter is reduced, as illustrated in Fig. 2(d-e). In the T-phase, the rotation angle goes abruptly to zero, whilst the tilting angle decreases abruptly across the R to T transition and decrease further with increasing compressive strain in the T-phase.

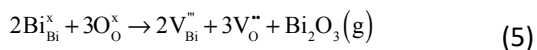
Compared to perfect structures, the presence of a Bi vacancy reduces the rotation angle in the R-phase, while a rotation of  $\sim 2.5^\circ$  is stabilized in the T-phase. However,  $\theta$  is identical in the R-phase for both stoichiometric and 12.5% Bi-vacancy BFO and decreases with increasing compressive strain. The opposite behaviour is observed upon entering the T-phase, where a decrease in tilting angle for a stoichiometric structure is obtained, whilst the tilting angle increases at the transition for the system with defects. A decreasing tilting angle upon increased strain in the T-phase can be understood from electrostatic repulsion between the two in-plane oxygen atoms, which repel each other more strongly upon removal of a Bi cation. Although the rotation and tilting patterns of the R- and T-phase is different, the local structural distortions around a Bi vacancy do not qualitatively change their  $aaa$  and  $aac^0$  Glazer tilt patterns<sup>11</sup>, respectively. Moreover, the effect of a Bi vacancy on the polarization components is small compared to stoichiometric BFO, as shown in Fig. 2(f). In general, the ferroelectric order of a high  $P_s$  and high  $T_c$  ferroelectric like BFO is robust with respect to point defects, while e.g. a “weak” ferroelectric like hexagonal  $\text{InMnO}_3$  is highly sensitive to point defects.<sup>53, 54</sup>

### 3.4 Strain dependence of formation energy of Bi-O vacancy pairs

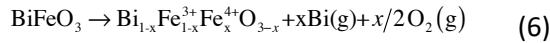
In sections 3.2 and 3.3 we studied Bi vacancies formed under oxygen rich conditions, where they are charge compensated by holes coupled to the formal oxidation of  $\text{Fe}^{3+}$  to  $\text{Fe}^{4+}$ . Under less oxygen rich conditions, Bi vacancies can be charge compensated by oxygen vacancies, described by



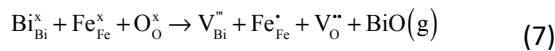
which in Kröger-Vink notation becomes:



We note that loss of Bi and O can also take place through the evaporation of gaseous elemental bismuth Bi (g) or gaseous bismuth suboxide BiO (g) together with O<sub>2</sub> (g),<sup>55</sup> but this will not affect the subsequent analysis. As reaction (5) results in five vacancies, we here choose a computationally friendly intermediate situation where one  $V_{\text{Bi}}^{\prime\prime\prime}$  is charge compensated by one hole and one  $V_{\text{O}}^{\bullet\bullet}$ .<sup>56</sup> This corresponds to mild hole doping of the Fe sub-lattice, with 1 out of every 8 Fe being formally oxidized to Fe<sup>4+</sup>, and a resulting stoichiometry of Bi<sub>0.875</sub>FeO<sub>2.958</sub>. The formation of a  $(V_{\text{Bi}} - V_{\text{O}})^{\prime}$  vacancy pair can then be described by the following reaction:



which in Kröger-Vink notation can be written as:



We note that there are two non-equivalent symmetry positions of oxygen atoms relative to the (001)-strain plane. Removing one of these two oxygen anions results either in an in-plane (IP) or an out-of-plane (OP) oriented Bi-O vacancy pair, with the axis between the vacant Bi and O being either close to parallel or perpendicular to the (001) strain plane, respectively, as shown in Fig. 3(b). These two different types of Bi-O vacancy pairs are considered in the following.

Introducing a vacancy-pair, two vacant sites cause larger structural distortions than one single Bi vacancy, rendering it difficult to classify relaxed defect structures as predominantly R- or T-phase. A small shift of the transition point from 4.5% to 4.4% compressive strain can still be inferred from the obtained discontinuity in vacancy pair formation enthalpy, as shown in Fig. 3(a). IP and OP Bi-O vacancy pairs behave differently across the R to T transition, whilst OP vacancy pairs are stabilized by 0.58 eV in the T-phase, IP vacancy pairs become strongly destabilized by 0.72 eV upon entering the T-phase. This abrupt change in vacancy pair formation enthalpy reflects the different shapes of the respective unit cells of the R- and T-phase. Vacancy pairs in the T-phase form more easily parallel to the elongated axis perpendicular to the strain plane as the elongated chemical bonds cost less energy to break than the relatively compressed IP bonds in. The calculated formation enthalpy for IP and OP vacancy pairs in unstrained bulk phase is 4.07 eV and 4.00 eV, respectively, indicating a preference for OP Bi-O vacancy pairs in the T-phase. Correspondingly we find that OP vacancy pairs are more stable in the R-phase, except in a narrow strain region between ~3.5 and 4.4% compressive strain.

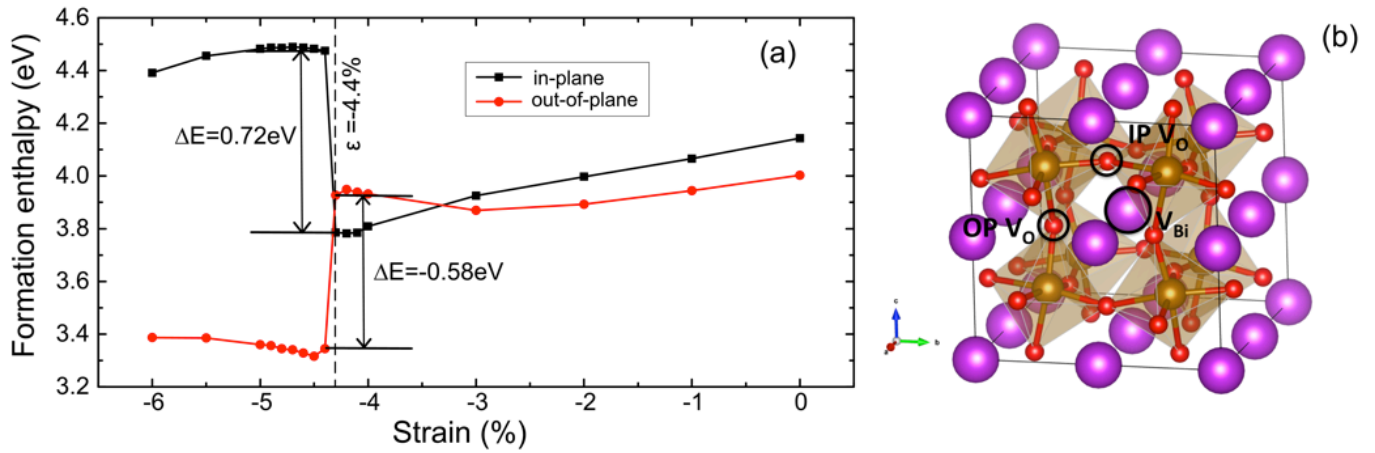


**Fig. 3** (a) Formation enthalpy of in-plane (black) and out-of-plane (red) Bi-O vacancy pairs as a function of strain; (b) Illustration of the two different types of Bi-O vacancy pairs.

### 3.5 Local structural response to Bi-O vacancy pairs under strain

To better understand the structural response of BFO to Bi-O vacancy pair formation, combined with the response to epitaxial strain, full geometry optimization calculations of unstrained bulk BFO 40 atom cells, having either IP or OP vacancy pairs, were performed and compared to the results of stoichiometric BFO and BFO with a single Bi vacancy, see Table 1.

Fully relaxed unstrained structures with IP and OP Bi-O vacancy pairs both display a lattice contraction as compared to stoichiometric bulk. Also, the  $c/a$  ratio in cells with IP and OP vacancy pair is less than unity, albeit from different factors. Having an IP vacancy pair, the out-of-plane lattice parameter decreases substantially, while the in-plane lattice parameters remain almost unchanged. However, cells with an OP vacancy pair, display a significant contraction of the in-plane lattice parameters. Also, IP vacancy pairs are robust with respect to changes in the in-plane lattice parameters and can hence reduce out-of-plane contraction. OP vacancy pairs are, however, more sensitive to variations in the in-plane lattice parameter.

Both IP and OP Bi-O vacancy pairs impede polar cation displacements, see Fig. 4. Interestingly, the most significant differences in cation displacements does not occur close to the R to T transition, but at  $\sim 3\%$  compressive strain. The origin of the discontinuity in displacements, depicted in Fig. 4(c-d), can be related to an increase in formation enthalpy of in-plane vacancy pairs at about  $-3\%$ , as shown in Fig. 3(a). At this strain value, the out-of-plane rotation of the oxygen octahedra changes from in-phase to out-of-phase. The octahedral rotations remain out-of-phase also for compressive strain exceeding  $4.3\%$ , where the formation enthalpy is discontinuous. This can be rationalized from a steric point of view: an IP

vacancy pair results in more in-plane space than an OP vacancy pair, hence allowing the  $\text{FeO}_6$  octahedra to fill the vacant space by a rotation instead of a polar displacement.

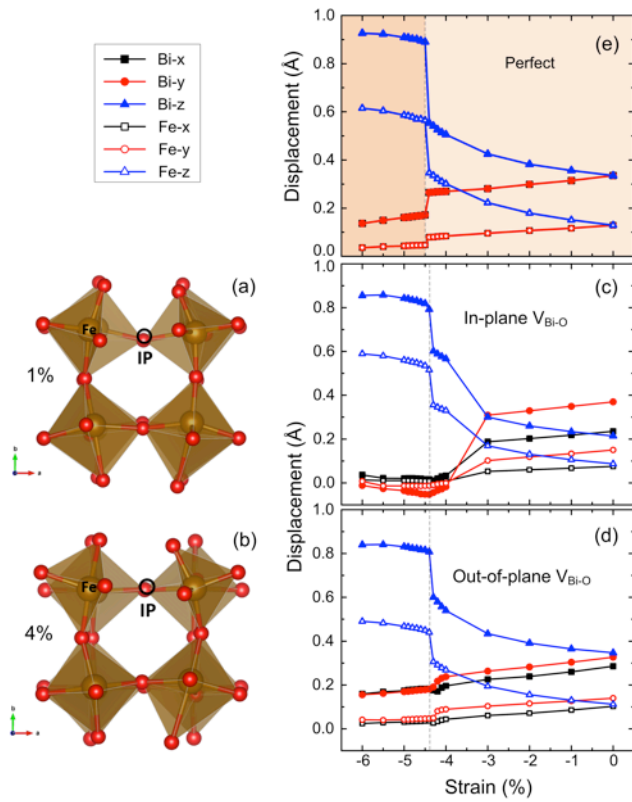


**Fig. 4** Relaxed structures including in-plane vacancy pairs showing the out-of-plane (along  $z$ ) rotation of oxygen octahedra under (a) 1% compressive strain displaying in-phase rotation of  $\text{FeO}_6$  and (b) 4% compressive strain displaying out-of-phase rotation of  $\text{FeO}_6$ . The displacement of Bi and Fe atoms relative to the oxygen sublattice for (c) in-plane Bi-O vacancy pairs (d) out-of-plane Bi-O vacancy pairs and (e) the perfect reference structure.

### 3.6 Polarization response to vacancies under strain

Next, we analyze the influence of different type of point defects on the ferroelectric polarization of BFO, using the point charge model to investigate the semi-quantitative effect of strain and point defects, while recognizing that the true polarization values will be systematically larger. Comparing the IP and OP polarization with the total polarization along  $[111]_{\text{pc}}$ , it is evident that a Bi vacancy alone has little impact on the polarization, whilst an IP Bi-O vacancy pairs reduces the polarization more than an OP vacancy pair, see Fig. 5. The in-plane polarization component for both types of vacancy pairs is reduced, while the IP vacancy pair suppresses the out-of-plane polarization strongly compared to the OP vacancy pair, which enhances the out-of-plane polarization. This suggests not only a strong driving force for ordering of the vacancy pairs in an OP alignment, but also that an applied electric field between a top and bottom electrode will favour OP ordering.

The increased out-of-plane polarization in the T-phase is suppressed by both IP and OP vacancy pairs, while the R-phase is less sensitive to IP vacancy pairs. In the R-phase both types of vacancy pair reduce the in-plane polarization component, while only subtly affecting the out-of-plane component, as illustrated in Fig 5.

Due to the compression and enhancement of in-plane and out-of-plane polarization components, the polarization vector will change from  $[111]_{pc}$  to nearly  $[001]_{pc}$ . This rotation occurs along the  $(110)$  plane in stoichiometric  $\text{BiFeO}_3$ . Angles between  $[001]_{pc}$  and the polarization vector in the “T-phase” at 4.5% compressive strain are shown in Figure 6. The angle between the OP  $[001]_{pc}$  direction and the polarization vector in the T-phase at 4.5% compressive strain depends strongly on the presence of point defects. In the T-phase this angle is  $8.2^\circ$  with a bismuth vacancy and  $2.7^\circ$  and  $14.1^\circ$  for IP and OP Bi-O vacancy pairs, respectively. IP vacancy pairs yield the smallest deviation in the polarization vector with respect to  $[001]_{pc}$ , while OP vacancy pairs give the largest angle between the  $[001]_{pc}$  direction and the resulting polarization vector.

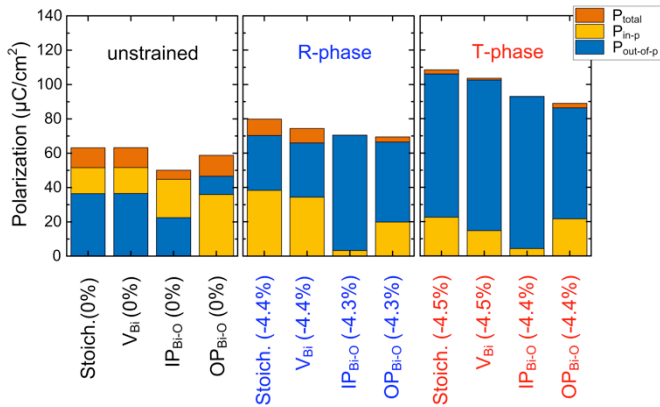


**Fig. 5** Point charge calculated polarization of  $\text{BiFeO}_3$  in the R- and T-phase with the three different defects considered in this work. The blue and brown bars **labelled** Pout-of-p and Pin-p show the out-of-plane and in-plane components of the total polarization, respectively, while the orange bar shows the polarization along the  $[111]_{pc}$ .

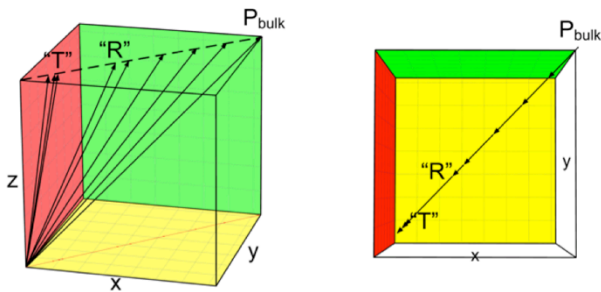


**Fig. 6.** Schematic illustration of how compressive strain induces a polarization rotation in stoichiometric  $\text{BiFeO}_3$  (left), and projection of the overall polarization onto the  $(001)$  plane (right).

### 3.7 Effect of vacancies on the electronic properties

Finally, we turn to the effect of point defects on the electronic densities of states (DOS) of unstrained bulk  $\text{BiFeO}_3$ , as presented in Fig. 7. Our calculated DOSs agree well with previous reports.<sup>10, 34, 38, 39, 57</sup> Both single Bi vacancies and an OP Bi-O vacancy pairs are expected to give rise to p-type conductivity, as the Fermi energy is then situated just below the top of the valence band. Bi vacancies and IP vacancy pairs, however, results in deep gap states composed of Fe 3d and O 2p, but not OP vacancy pairs. In contrast to the effect of Bi vacancies and OP vacancy pairs, the insulating nature of BFO is retained under the presence of IP vacancy pairs, but with a significant reduction of the band gap from 2.32eV to 1.31eV.

Moving to examine the DOSes of strained structures we find that epitaxial strain only subtly affects the electronic structure of stoichiometric cells, as illustrated in Figure 8(a-d).

However, with the presence of single Bi vacancies, compressive strain moves the valence band maximum below the Fermi level and restores insulating behavior. The impurity state just above the Fermi level is a mixed state of Fe 3d and O 2p, which splits into two bands across the R to T the phase transition. IP and OP vacancy pairs under 4.3% compressive strain give rise to very similar electronic structures. The main difference is that in the T-phase, at -4.4% strain, the mixed Fe-O state is much wider in energy for OP vacancy pairs than for IP vacancy pairs, indicating more orbital overlap between the Fe 3d and O 2p orbitals with OP- than IP- vacancy pairs.

Our results shed light on the complex interplay between Bi deficiency, strain, and electronic conductivity. While p-type conductivity is observed in bulk ceramics for high  $p_{\text{O}_2}$ ,<sup>58</sup> where Bi vacancies are favoured relative to Bi-O vacancy pairs, strain may alter the relationship between Bi deficiency, strain, and electronic conductivity in epitaxial thin films. Compared to bulk ceramics, the equilibration time for diffusion processes, e.g. loss of volatile bismuth or reversible exchange of oxygen with atmosphere, is much shorter for nanometer thick films than micrometer to millimeter thick ceramics.<sup>18,26</sup> This implies that single Bi vacancies can rapidly be charge compensated by holes or oxygen vacancies even at low temperatures, implying that polarization and electrical conductivity can be quickly tuned by post-synthesis annealing affecting the oxygen vacancy level.

We note that local strain fields surround ferroelectric and ferroelastic domain walls, which will affect the local defect levels and promote local Bi deficiency.<sup>27</sup> Atmosphere-controlled annealing can thus tune the domain walls between conducting and insulating states. Understanding the interplay between strain, point defects and functional properties is thus imperative to design the properties of both thin films and ferroelectric domain walls.

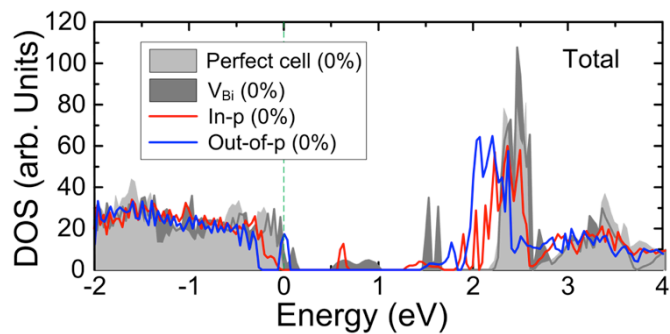


**Fig. 7** Total electronic densities of states (DOS) of stoichiometric bulk  $\text{BiFeO}_3$ , and unstrained BFO with a Bi vacancy, an IP Bi-O vacancy pair and an OP Bi-O vacancy pair.

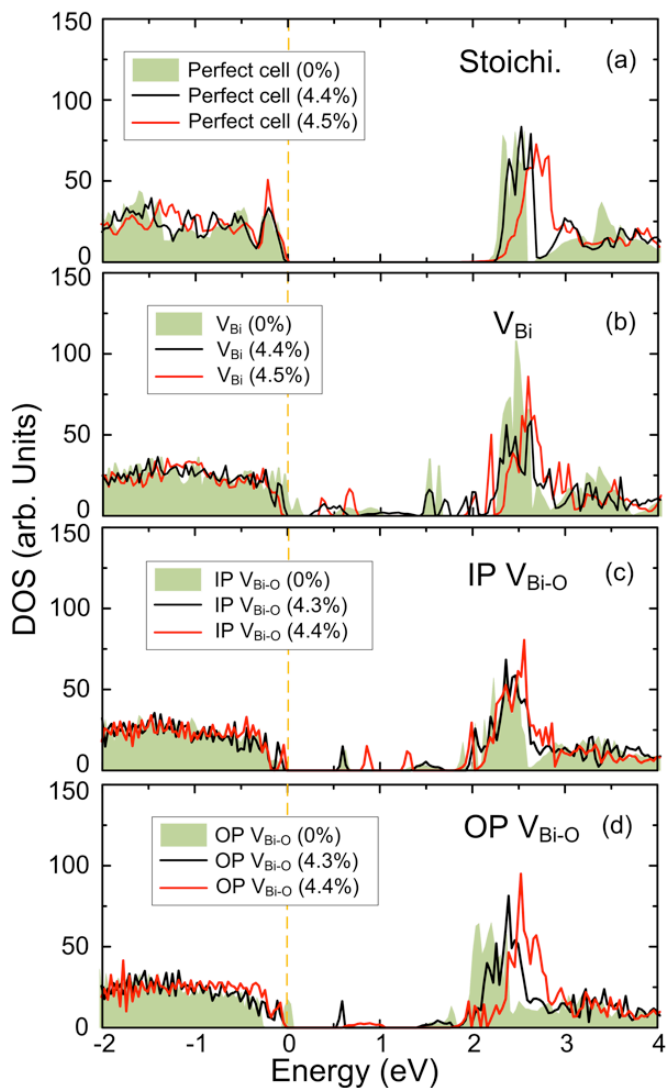


**Fig. 8.** Total electronic densities of states (DOS) of  $\text{BiFeO}_3$  with different strain levels for (a) stoichiometric material, (b) Bi vacancies, (c) IP Bi-O vacancy pairs and (d) OP Bi-O vacancy pair.

## 4 Conclusions

In summary, we have investigated the energetics of Bi vacancies and Bi-O vacancy pairs in (001)-strained BiFeO<sub>3</sub> thin films. The Bi vacancy enthalpy of formation decreases with increasing compressive strain up to  $\sim$ -3.5%, then increases with further compressive strain, before dropping abruptly at the transition from rhombohedral R-phase to tetragonal T-phase. The stability of bismuth-oxygen vacancy pairs increases monotonically with compressive strain up to  $\sim$ -3%. In the R-phase in-plane (IP) oriented vacancy pairs are more stable than out-of-plane (OP) oriented for less strain than -3%, while the situation reverses for the strain range between  $\sim$ -3% and -4.5% where the R- to T-phase transition takes place. Upon entering the T-phase, OP oriented vacancy pairs are strongly preferred over IP oriented by more than 1 eV. The calculated spontaneous polarization is insensitive to single Bi vacancies, while IP vacancy pairs reduce the IP polarization components, yielding a net polarization direction close to [001]. IP vacancy pairs under small strain levels cause local in-phase octahedral rotations in contrast with the anti-phase rotations of the stoichiometric bulk material. Bi deficiency is predicted to give p-type conductivity, in agreement with recent experimental work on thin films, domain walls and bulk ceramics, highlighting the importance of cation non-stoichiometry in BiFeO<sub>3</sub>.

**Table 1.** Structural parameters for unstrained bulk BiFeO<sub>3</sub>, with Bi vacancies ( $V_{\text{Bi}}$ ) and Bi-O vacancy pairs ( $V_{\text{Bi-O}}$ ) oriented in-plane (IP) and out-of-plane (OP).

	Bulk	$V_{\text{Bi}}$	$V_{\text{Bi-O}}$ (IP)	$V_{\text{Bi-O}}$ (OP)
$a$ (Å)	7.884	6.734	7.884	7.847
$b$ (Å)	7.884	6.734	7.884	7.859
$c$ (Å)	7.884	7.820	7.736	7.77
$c/a$	1.00	1.16	0.98	0.99
$\alpha$ (°)	89.56	89.23	89.56	89.22
$\beta$ (°)	89.56	89.23	89.56	89.60
$\gamma$ (°)	89.56	89.23	89.56	89.43
$V$ (Å <sup>3</sup> )	489.97	478.07	480.80	479.09

## Conflicts of interest

There are no conflicts to declare.

## Acknowledgments

Financial support from the Research Council of Norway through project no. 231430 and computational resources provided by Sigma2 Uninett through project no. NN9264K are acknowledged.

## Notes and references

1. G. Catalan, J. F. Scott, *Adv Mater.* 2009, 21, 2463-2485.
2. J. Wang, J. B. Neaton, H. Zheng, V. Nagarajan, S. B. Ogale, B. Liu, D. Viehland, V. Vaithyanathan, D. G. Schlom, U. V. Waghmare, N. A. Spaldin, K. M. Rabe, M. Wuttig, R. Ramesh, *Science*. 2003, 299, 1719-1722.
3. I. C. Infante, S. Lisenkov, B. Dupe, M. Bibes, S. Fusil, E. Jacquet, G. Geneste, S. Petit, A. Courtial, J. Juraszek, L. Bellaiche, A. Barthelemy, B. Dkhil, *Phys. Rev. Lett.*, 2010, 105, 057601.
4. H. W. Jang, D. Ortiz, S. H. Baek, C. M. Folkman, R. R. Das, P. Shafer, Y. Chen, C. T. Nelson, X. Pan, R. Ramesh, C. B. Eom, *Adv. Mater.*, 2009, 21, 817.
5. J. F. Li, J. L. Wang, M. Wuttig, R. Ramesh, N. Wang, B. Ruetter, A. P. Pyatakov, A. K. Zvezdin, D. Viehland, *Appl. Phys. Lett.*, 2004, 84, 5261-5263.
6. C. Ederer, N. A. Spaldin, *Phys. Rev. Lett.*, 2005, 95, 257601.
7. L. R. Dedon, S. Saremi, Z. H. Chen, A. R. Damodaran, B. A. Apgar, R. Gao, L. W. Martin, *Chem. Mater.*, 2016, 28, 5952-5961.
8. A. Lahmar, K. Zhao, S. Habouti, M. Dietze, C. H. Solterbeck, M. Es-Souni, *Solid State Ionics*. 2011, 202, 1-5.
9. F. Kubel, H. Schmid, *Acta Crystallogr.*, 1990, 46, 698-702.
10. J. B. Neaton, C. Ederer, U. V. Waghmare, N. A. Spaldin, K. M. Rabe, *Phys. Rev. B*. 2005, 71, 014113.
11. A. M. Glazer, *Acta Crystallogr.*, 1972, B 28, 3384-&.
12. H. D. Megaw, C. N. W. Darlington, *Acta Crystallogr.*, 1975, A 31, 161-173.
13. R. J. Zeches, M. D. Rossell, J. X. Zhang, A. J. Hatt, Q. He, C. H. Yang, A. Kumar, C. H. Wang, A. Melville, C. Adamo, G. Sheng, Y. H. Chu, J. F. Ihlefeld, R. Erni, C. Ederer, V. Gopalan, L. Q. Chen, D. G. Schlom, N. A. Spaldin, L. W. Martin, R. Ramesh, *Science*. 2009, 326, 977-980.
14. A. J. Hatt, N. A. Spaldin, C. Ederer, *Phys. Rev. B*. 2010, 81, 054109.
15. H. Bea, B. Dupe, S. Fusil, R. Mattana, E. Jacquet, B. Warot-Fonrose, F. Wilhelm, A. Rogalev, S. Petit, V. Cros, A. Anane, F. Petroff, K. Bouzehouane, G. Geneste, B. Dkhil, S. Lisenkov, I. Ponomareva, L. Bellaiche, M. Bibes, A. Barthelemy, *Phys. Rev. Lett.*, 2009, 102, 217603.
16. H. M. Christen, J. H. Nam, H. S. Kim, A. J. Hatt, N. A. Spaldin, *Phys. Rev. B*. 2011, 83, 144107.
17. J. B. Neaton, C. Ederer, U. V. Waghmare, N. A. Spaldin, K. M. Rabe, *Phys. Rev. B*. 2005, 71, 8.
18. S. V. Kalinin, N. A. Spaldin, *Science*. 2013, 341, 858-859.
19. Y. M. Kim, A. Morozovska, E. Eliseev, M. P. Oxley, R. Mishra, S. M. Selbach, T. Grande, S. T. Pantelides, S. V. Kalinin, A. Y. Borisevich, *Nat. Mater.*, 2014, 13, 1019-1025.
20. P. P. Biswas, C. Thirnal, S. Pal, P. Murugavel, *J. Appl. Phys.*, 2018, 123, 024101.
21. A. Ravalia, M. Vagadia, P. S. Solanki, S. Gautam, K. H. Chae, K. Asokan, N. A. Shah, D. G. Kuberkar, *J. Appl. Phys.*, 2014, 116, 153701.
22. U. Aschauer, R. Pfenninger, S. M. Selbach, T. Grande, N. A. Spaldin, *Phys. Rev. B*. 2013, 88, 054111.
23. A. Marthinsen, C. Faber, U. Aschauer, N. A. Spaldin, S. M. Selbach, *MRS Commun.*, 2016, 6, 182-191.
24. U. Aschauer, N. A. Spaldin, *Appl. Phys. Lett.*, 2016, 109, 031901.
25. U. Aschauer, N. Vonruti, N. A. Spaldin, *Phys. Rev. B*. 2015, 92, 054103.
26. T. Grande, J. R. Tolchard, S. M. Selbach, *Chem. Mater.*, 2012, 24, 338-345.
27. T. Rojac, A. Bencan, G. Drazic, N. Sakamoto, H. Ursic, B. Jancar, G. Tavcar, M. Makarovic, J. Walker, B. Malic, D. Damjanovic, *Nat. Mater.*, 2017, 16, 322.
28. T. Rojac, M. Kosec, B. Budic, N. Setter, D. Damjanovic, *J. Appl. Phys.*, 2010, 108, 074107.
29. M. I. Morozov, M. A. Einarsrud, T. Grande, *J. Appl. Phys.*, 2014, 115, 122905.
30. E. T. Wefring, M. A. Einarsrud, T. Grande, *Phys. Chem. Chem. Phys.*, 2015, 17, 9420-9428.
31. J. Y. Chen, Y. Wang, H. Wang, S. M. Zhang, Y. Deng, *Sci. Rep.*, 2016, 6, 19385.
32. S. J. Clark, J. Robertson, *Appl. Phys. Lett.*, 2009, 94, 022902.
33. S. Ju, T. Y. Cai, *Appl. Phys. Lett.*, 2009, 95, 231906.
34. T. Shimada, T. Matsui, T. Xu, K. Arisue, Y. J. Zhang, J. Wang, T. Kitamura, *Phys. Rev. B*. 2016, 93, 174107.
35. R. P. Yang, S. X. Lin, X. G. Fang, X. S. Gao, M. Zeng, J. M. Liu, *J. Appl. Phys.*, 2013, 114, 233912.
36. Z. Zhang, P. Wu, L. Chen, J. L. Wang, *Appl. Phys. Lett.*, 2010, 96, 232906.

37. L. Y. Zou, R. P. Yang, Y. B. Lin, M. H. Qin, X. S. Gao, M. Zeng, J. M. Liu, *J. Appl. Phys.*, 2013, 114, 034105.
38. B. Jiang, S. M. Selbach, *J Solid State Chem.* 2017, 250, 75-82.
39. T. R. Paudel, S. S. Jaswal, E. Y. Tsybal, *Phys. Rev. B.* 2012, 85, 104409.
40. I. MacLaren, L. Q. Wang, B. Schaffer, Q. M. Ramasse, A. J. Craven, S. M. Selbach, N. A. Spaldin, S. Miao, K. Kalantari, I. M. Reaney, *Adv. Funct. Mater.*, 2013, 23, 683-689.
41. P. E. Blochl, *Phys. Rev. B.* 1994, 50, 17953-17979.
42. G. Kresse, J. Furthmuller, *Phys. Rev. B.* 1996, 54, 11169-11186.
43. G. Kresse, D. Joubert, *Phys. Rev. B.* 1999, 59, 1758-1775.
44. J. P. Perdew, A. Ruzsinszky, G. I. Csonka, O. A. Vydrov, G. E. Scuseria, L. A. Constantin, X. L. Zhou, K. Burke, *Phys. Rev. Lett.*, 2008, 100, 136406.
45. V. I. Anisimov, J. Zaanen, O. K. Andersen, *Phys. Rev. B.* 1991, 44, 943-954.
46. S. L. Dudarev, G. A. Botton, S. Y. Savrasov, C. J. Humphreys, A. P. Sutton, *Phys. Rev. B.* 1998, 57, 1505-1509.
47. N. A. Spaldin, *J Solid State Chem.* 2012, 195, 2-10.
48. J. M. Rondinelli, N. A. Spaldin, *Adv. Mater.*, 2011, 23, 3363-3381.
49. A. Jain, G. Hautier, S. P. Ong, C. J. Moore, C. C. Fischer, K. A. Persson, G. Ceder, *Phys Rev B.* 2011, 84, 045115.
50. Y. Meng, X. W. Liu, C. F. Huo, W. P. Guo, D. B. Cao, Q. Peng, A. Dearden, X. Gonze, Y. Yang, J. G. Wang, H. J. Jiao, Y. W. Li, X. D. Wen, *J. Chem. Theory Comput.*, 2016, 12, 5132-5144.
51. M. Avdeev, E. N. Caspi, S. Yakovlev, *Acta Crystallogr.*, 2007, B63, 363-372.
52. N. W. Thomas, A. Beitollahi, *Acta Crystallogr.*, 1994, B50, 549-560.
53. F. T. Huang, X. Wang, Y. S. Oh, K. Kurushima, S. Mori, Y. Horibe, S. W. Cheong, *Phys. Rev. B.* 2013, 87, 184109.
54. S. M. Griffin, M. Reidulff, S. M. Selbach, N. A. Spaldin, *Chem. Mater.*, 2017, 29, 2425-2434.
55. S. M. Selbach, T. Tybell, M. A. Einarsrud, T. Grande, *J Solid State Chem.* 2010, 183, 1205-1208.
56. L. Xia, T. Tybell, S. M. Selbach, *Submitted.*, 2018, , .
57. R. Saeterli, S. M. Selbach, P. Ravindran, T. Grande, R. Holmestad, *Phys. Rev. B.* 2010, 82, 064102.
58. N. Maso, A. R. West, *Chem. Mat.*, 2012, 24, 2127-2132.